國 立 交 通 大 學

物理研究所

碩士論文

比較兩種取得光電倍增管增益的方法

Comparing the gains of a photomultiplier tube between two methods

研 究 生：陳郃諺

指導教授：林貴林　教授

中 華 民 國 一 百 零 二 年 一 月

比較兩種取得光電倍增管增益的方法

Comparing the gains of a photomultiplier tube between two methods

研 究 生 ： 陳郃諺　　Student: Ho-Yen Chen

指導教授 ： 林貴林　　Advisor: Guey-Lin Lin

國 立 交 通 大 學

物 理 研 究 所

碩 士 論 文

A Thesis

Submitted to Institute of Physics

National Chiao Tung University

in Partial Fulfillment of the Requirements

for the Degree of

Master

In

Physics

January, 2013

Hsinchu City, Taiwan, Republic of China

中華民國一百零二年一月

比較兩種取得光電倍增管增益的方法

研 究 生 ： 陳郤諺　　指導教授 ： 林貴林

國立交通大學物理研究所

摘　　要

近年來，液態閃爍體探測器廣泛地應用於大型粒子探測器當中，如大亞灣微中子實驗。此類探測器多使用光電倍增管捕捉訊號及放大。其增益的程度與計算粒子能量有密切的關係，因此對其增益的校正及監控對實驗數據的可信度佔有關鍵的因素。在大亞灣實驗當中使用兩種校正及監控光電倍增管增益的方法－無光噪音及發光二極體光源。本論文比較在此兩種方法下取得的光電倍增管增益的差異程度。

Comparing the gains of a photomultiplier tube between two methods

Student: Ho-Yen Chen Advisor: Guey-Lin Lin

Institute of Physics

National Chiao Tung University

ABSTRACT

Recently, liquid scintillation detectors are extensively used with particle detectors in many projects such as Dayabay. Mostly in such detectors, photomultiplier tubes (PMTs) are used for the detection of light. The gains of PMTs have closely relation with the calculation for particle energy, so it is crucial for calibrating the gains of PMTs. Such as Daya-bay, there are two methods, Dark noise and LED light, to get the gains of PMTs. In this thesis, we discuss the discrepancy in the two methods.

致　謝

感謝指導教授林貴林老師讓我有機會參與大亞灣計畫，從中學習與體認到許多關於大型物理實驗的趣味與奧妙之處，並且在研究方面非常細心的指引。感謝葉永順學長在實驗方面不斷的幫助且花許多時間跟我耐心的討論，以及胡貝禎學姐的許多建議。感謝林彥勳常在課業與研究上常討論解答物理方面的問題。感謝林秉言分擔在研究上的人力需求。

Contents

List of Figures

List of Tables

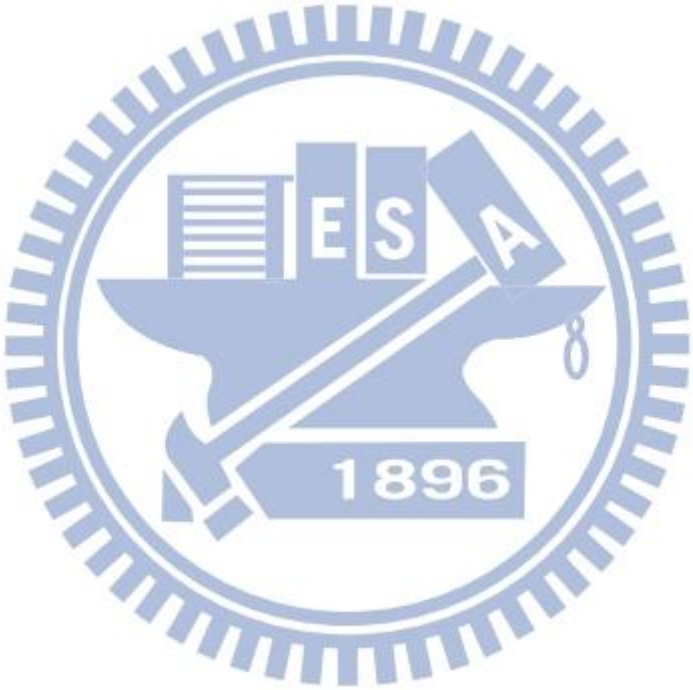

Chapter 1

Introduction

1.1 Neutrinos

In the early twentieth century, the beta-decay was thought to be mono-energetic because it is a two-body decay into proton and electron. Nevertheless, J. Chadwick showed that the beta-ray spectrum was continuous. Fig. 1.1 shows the typical beta-ray energy distribution curve. Later, Pauli postulated a tiny neutral particle, which we call neutrino today. This particle carries away some energy in the three-body beta-decay process[1]. Unfortunately, the neutrino cannot be observed directly. Only the products from its interaction with matter can be observed. The first detection of neutrinos was made in 1956, now known as the Cowan-Reines neutrino experiment, where the antineutrinos created in nuclear reactor by beta decay interacted with protons producing positrons and neutrons. In 1962, it was demonstrated that more than one type of neutrino exist by first detecting interactions of the muon neutrino. The first detection of tau neutrino interactions was announced in 2000. Hence there are three flavors of neutrinos: electron neutrino ν_e, muon neutrino ν_μ and tau neutrino ν_τ. The particular neutrino flavors are associated to the observed lepton type[1].

Starting in the late 1960s, several experiments found that the number of electron neutrinos arriving from the sun was about one-third the number predicted by standard solar model. This discrepancy, which became known as the solar neutrino problem, remained unresolved for some thirty years. It was resolved by the discovery of neutron oscillation phenomenon which imply neutrrinos are massive [1].

Starting in 1998, experiments began to show that solar and atmospheric neutrinos change flavors. This resolved the solar neutrino problem: the electron neutrinos produced in the Sun had partly changed into other flavors which the experiments could not detect. Neutrinos are massless in the standard model of

particle physics. However, neutrino oscillation experiments in the past decade have indicated that it is massive. Since neutrinos have masses with small splittings so that different flavors of neutrinos can mix quantum mechanically and show oscillation behavior[1].

Neutrino oscillation arises from a mixture between the flavor and mass eigenstates of neutrinos. That is, the three neutrino states that interact with the charged leptons in weak interactions are each a different superposition of the three neutrino states of definite mass. Neutrinos are created in weak decays and interact in their flavor eigenstates. The unitary transformation relating the flavor and mass eigenstates can be written as

$$|\nu_\alpha\rangle = \sum_i^\alpha U_{\alpha i} |\nu_i\rangle \ ,$$

where $|\nu_\alpha\rangle$ is a neutrino with definite flavor. α=electron, muon or tau. $|\nu_i\rangle$ is a neutrino state with definite mass m_i. i=1,2 or 3. $U_{\alpha i}$ represents the Pontecorvo–Maki–Nakagawa–Sakata matrix. When the standard three neutrino scenario is considered, the matrix is 3×3.

$$U = \begin{pmatrix} U_{e1} & U_{e2} & U_{e3} \\ U_{\mu 1} & U_{\mu 2} & U_{\mu 3} \\ U_{\tau 1} & U_{\tau 2} & U_{\tau 3} \end{pmatrix}$$

$$= \begin{pmatrix} 1 & 0 & 0 \\ 0 & c_{23} & s_{23} \\ 0 & -s_{23} & c_{23} \end{pmatrix} \begin{pmatrix} c_{13} & 0 & s_{13}e^{i\delta} \\ 0 & 1 & 0 \\ -s_{13}e^{i\delta} & 0 & c_{13} \end{pmatrix} \begin{pmatrix} c_{12} & s_{12} & 0 \\ -s_{12} & c_{12} & 0 \\ 0 & 0 & 1 \end{pmatrix} \begin{pmatrix} e^{i\alpha_1/2} & 0 & 0 \\ 0 & e^{i\alpha_2/2} & 0 \\ 0 & 0 & 1 \end{pmatrix}$$

$$= \begin{pmatrix} c_{12}c_{13} & s_{12}c_{13} & s_{13}e^{-i\delta} \\ -s_{12}c_{23} - c_{12}s_{23}s_{13}e^{i\delta} & c_{12}c_{23} - s_{12}s_{23}s_{13}e^{i\delta} & s_{23}c_{13} \\ s_{12}s_{23} - c_{12}c_{23}s_{13}e^{i\delta} & -c_{12}s_{23} - s_{12}c_{23}s_{13}e^{i\delta} & c_{23}c_{13} \end{pmatrix} \begin{pmatrix} e^{i\alpha_1/2} & 0 & 0 \\ 0 & e^{i\alpha_2/2} & 0 \\ 0 & 0 & 1 \end{pmatrix}$$

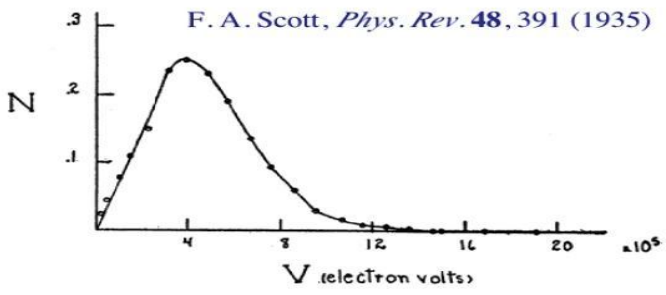

Fig. 1.1: Energy distribution curve of the beta-decays[2].

1.2 The Daya Bay neutrino oscillation experiment

Daya Bay experiment measures θ_{13} by using eight antineutrino detectors at three sites. The detectors measure the survival probability of reactor antineutrino produced by the reactors of Daya Bay nuclear power complex. The observed survival probability as a function of distance is given by

$$P_{sur} = \left|\left\langle \nu_e \middle| \nu_e(t) \right\rangle\right|^2 = 1 - \sin^2 2\theta_{13} \sin^2 \frac{\Delta m_{31}^2 L}{4E_\nu} - \cos^4\theta_{13} \sin^2 2\theta_{12} \sin^2 \frac{\Delta m_{21}^2 L}{4E_\nu} \quad (1.1)$$

The value of $\sin^2 2\theta_{13}$ can be determined by comparing the ratio of interaction rates in multiple detectors. This is demonstrated by the following equation.

$$\frac{N_f}{N_n} = \left(\frac{N_{p,f}}{N_{p,n}}\right)\left(\frac{L_n}{L_f}\right)^2 \left(\frac{\epsilon_f}{\epsilon_n}\right)\left[\frac{P_{sur}(E,L_f)}{P_{sur}(E,L_n)}\right] \quad (1.2)$$

, where N_f and N_n are measured rates at far site and near site respectively. $N_{p,f}$ and $N_{p,n}$ are detector masses at far site and near site, respectively. L_n and L_f are distances to near site and far site respectively. ϵ_f and ϵ_n are detector efficiencies at far site and near site respectively. E and L_f /L_n in P_{sur} are associated with E_ν and L in Eq1.1 respectively. There are eight antineutrino detectors (AD) placed at Daya Bay underground laboratory. There are two near sites, Daya Bay near site and Ling Ao near site. Two ADs are placed at each near site. The other four ADs are placed at the far site for increasing the statistics. The experimental layout is shown in Fig. 1.2.

Each site is located adjacent to mountainous terrain, ideal for installing underground detectors that are well shielded from external backgrounds like cosmic-ray muons which are the main background to the Daya Bay experiment. Futhermore, background due to the muon spallation products at the depths of experiment halls and ambient gamma-background due to the radioactivity of the rock surrounding experiment halls are reduced by shielding the ADs with 2.5 meter of water. This water shielding also attenuates the flux of neutrons produced outside the water pool. Events with a pair of muons passing through the water in the water pool less than 200 μs apart have a small but finite probability to create a fake signal event. The time window 200 μs is the typical time window between a prompt signal due to positron annihilation and a delayed signal due to capture of neutron of an inverse beta-decay process.

There is a layer of Resistive Plate Chambers (RPC) above the water pool and 8” PMTs surrounding the water pool for the Cherenkov detection of muons. The setup is shown in Fig. 1.3.

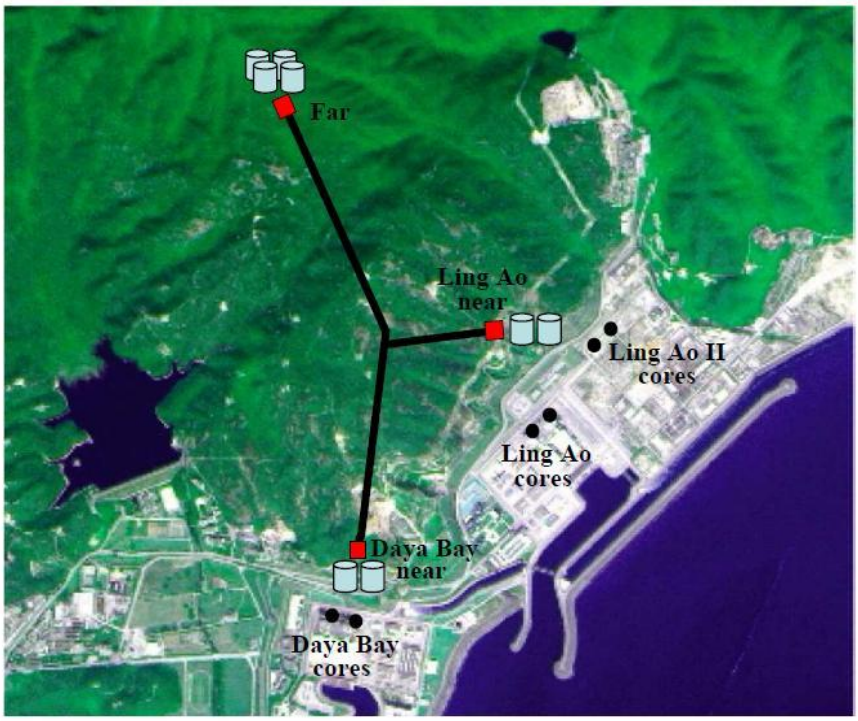

Fig. 1.2: The AD positions at Daya Bay[3].

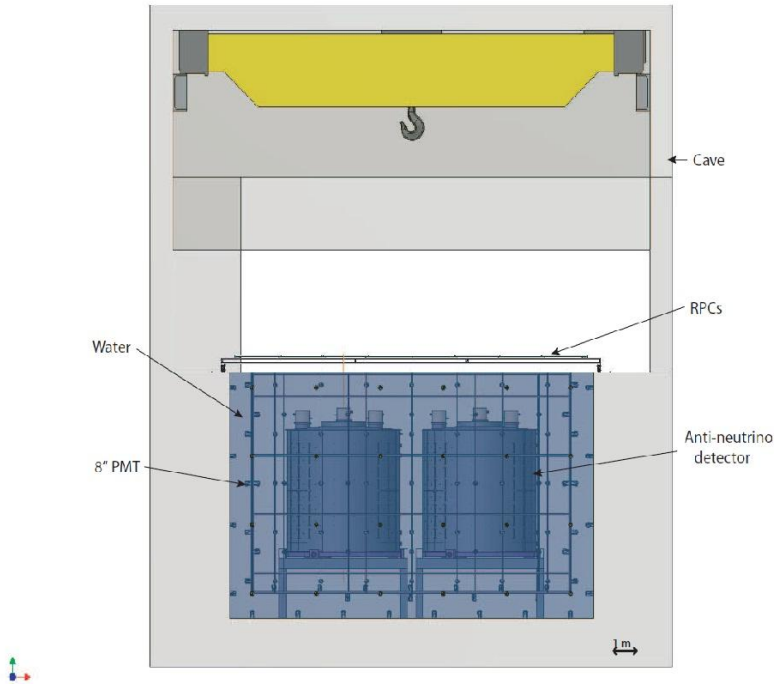

Fig. 1.3: Elevation view of an experiment hall, showing the water pool to shield backgrounds from muons, muon-induced neutrons and radioactivity of rock[3].

1.3 The Daya Bay antineutrino detector

The Daya Bay antineutrino detector is a three zone detector as shown in Fig. 1.4. The outermost zone is the mineral oil buffer surrounded by 192 8" PMTs. The second zone is the gamma catcher, which is liquid scintillator only. The innermost zone is the antineutrino target, which is 0.1% gadolinium-doped liquid scintillator. The detection process is the inverse beta-decay[12].

$$\overline{\nu}_e + p \rightarrow e^+ + n \tag{1.3}$$

The positrons annihilate soon after generated by the inverse beta-decay and produce gamma rays which could be observed by PMTs. This is the so-called prompt signal. The neutrons will go through thermal scattering process and finally captured by nucleus, namely protons or Gd. When a neutron is captured by nucleus, gamma rays are emitted, which is the so-called delayed signal comparing to the positron annihilation. If the neutron is captured by a proton, a 2.2MeV gamma-ray is emitted for each event[12],i.e.

$$n + p \rightarrow D + \gamma(2.2MeV) \tag{1.4}$$

However the cross section of the neutron captured by a proton is only 0.3b. To enhance the neutron capture probability, a 0.1% Gd is doped in the liquid scintillator. The cross section of neutron captured by Gd is 49000b. The Gd will be excited after capturing neutrons and goes back to the ground state by emitting 8 MeV gamma rays[3][12],i.e.

$$n + Gd \rightarrow Gd^* \tag{1.5}$$

$$Gd^* \rightarrow Gd + \gamma(8MeV) \tag{1.6}$$

The scheme of the detection mechanism based on inverse beta-decay is shown in Fig. 1.5. The prompt and delayed signals are both time-tagged signals. Together with the energy-tagged signals, the inverse beta-decay in 0.1% Gd-doped liquid scintillator is a good tool to suppress background events.

The neutrons are neutral particles so that the direct detection is difficult. A large mass antineutrino detector should be in the order of tons. For the simplicity of simulation and analysis, the cylindrical detector shape is chosen. There are external backgrounds like muon-induced neutrons, radioactivity of

PMT glasses, natural radioactivity of rock, etc. The mineral oil is used for the antineutrino detectors to be a buffer for the detection of scintillation light. Three-zone detector design is chosen to have better energy resolution. The innermost GdLS is 20 tons and the outer layer is another 20 tons of the pure scintillator. The outermost layer is 40 tons mineral oil. 192 8" R5912 Hamamatsu PMTs are mounted on the inner surface of the stainless steel tank in eight horizontal rings, viewing the target volume and the gamma catcher. The cross-sectional model of an AD is shown in Fig. 1.6[3][12].

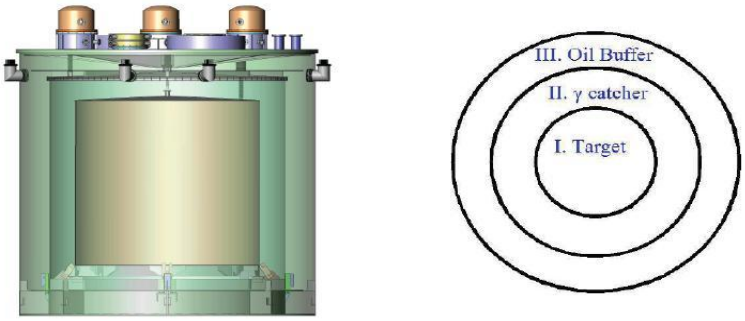

Fig. 1.4: Three zone structure of Daya Bay antineutrino detector. Left: Transparent cross-section of the antineutrino detector. Right: Schematic top view of the three different zones of the AD.

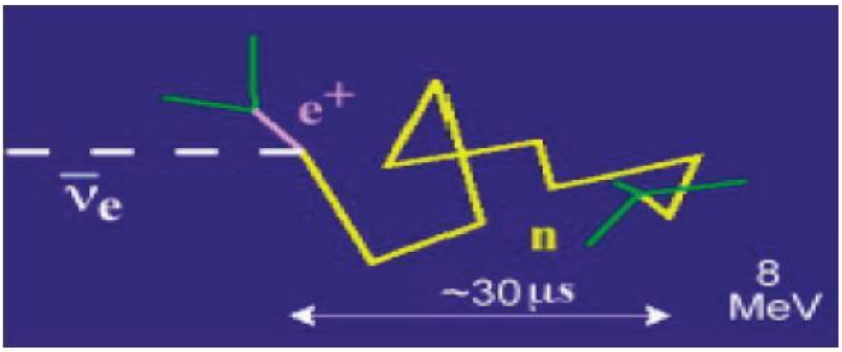

Fig. 1.5: Daya Bay AD detection mechanism based on inverse beta-decay.

1.4 The inner acrylic vessel

In the aspect of hardware, Taiwan group is responsible for the inner acrylic vessels (IAVs). IAVs are produced by Nakano Inc. Co. in Taiwan. It was my part of works to help and supervise Nakano to pro-

duce the IAVs. The first standard process is to produce an IAV to measure the transmittance of acrylic samples that ensure the acryl is the UV-transparent type. After Nakano making the varied shapes of the acrylic panels, three kinds of processes are performed on acryl: polishing, bonding, annealing, including heating the panels to shape them. Polish affects the optical behavior. Finer polish enhances the specular reflection and ensure that light goes more straightly when passing through the acrylic panels, namely reducing diffuse reflection. When bonding these panels, a commercial secret glue was used and it needs a so-called UV curing process. The bonding area is composing of acrylic panels and glue, and exposed to UV lamps at 365nm. To cure a 2mm thick bonding area, a 10W UV lamp is needed to irradiate the area for around 2 days, depending on the manufacture status of glue and thickness of acrylic panels.

The inner space of IAVs requires a cleaning process before bonding the top lid, because the IAVs would not be opened anymore except the calibration ports. Fig. 1.7 shows the overview of cleaning process. The whole process was performed in the cleaning room. The requirements for cleanliness are no metal dust, no chemical left, no general dirt like finger print, and as few as possible dust. The tolerance amount of dust confined in the IAV is less than 25mg.

1% Alconox and deionized water were used to clean IAVs. The resistance of deionized water should be greater than 18MΩ-cm. To confirm that the Alconox solution is removed by deionized water, conductivity of the washdown water should be smaller than 1μS/cm after cycle rinse.

After cleaning the IAV, we packed it in a wooden box and the space was filled with styrofoam. We then transport the whole package to Daya Bay by ship. The unpacking and cleaning were done on site. If there is no critical damage such as scratch, dirt or bubble in the IAV, we installed the IAV in AD.

I also took the shift on site, did cabling in the electrical room and helped to install the ACU system. I also carried out other tasks whenever manpower is needed.

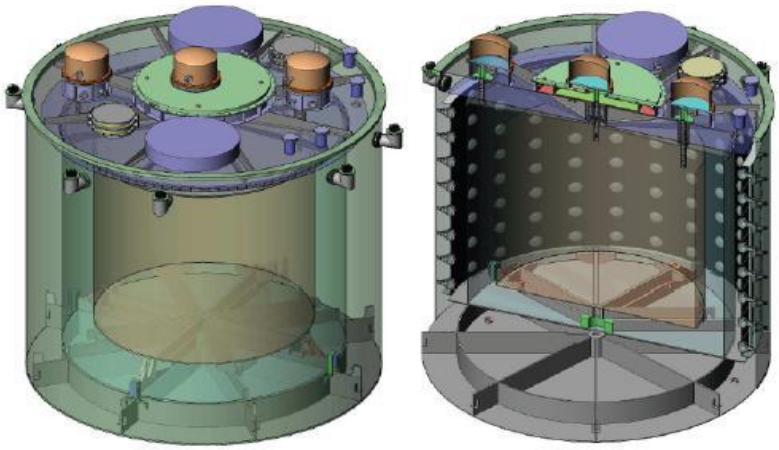

Fig. 1.6: The cross-sectional view of the AD. The pictures show complete AD including calibration boxes and overflow tanks on the top of the AD.

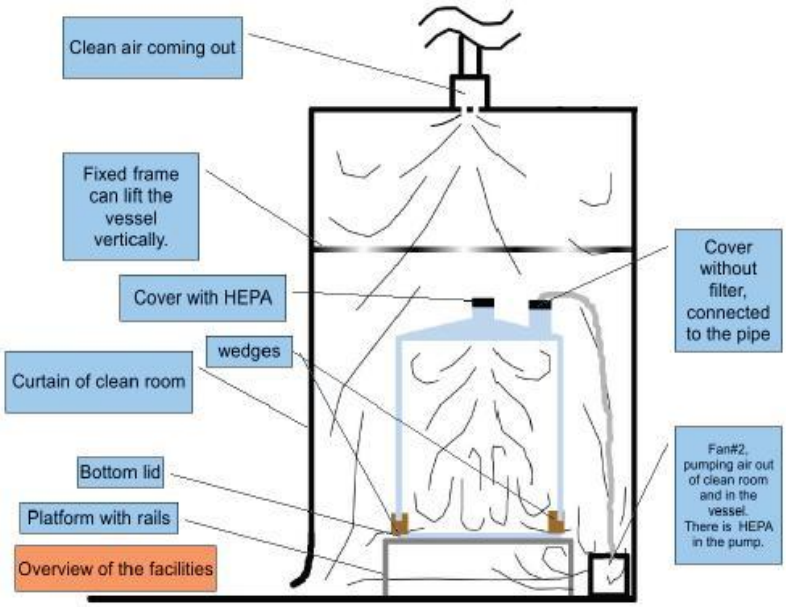

Fig. 1.7: The overview of cleaning facilities.

Chapter 2

Photomultiplier tubes and the response function

In this chapter, I discuss some basic properties of photomultiplier tubes and response function. I will not discuss the design details such as the material of cathode, efficiency of different tube geometry, etc. I simply introduce the general formula and properties of photomultiplier tubes.

2.1 Basic principles of photomultiplier tubes

A photomultiplier tube is a vacuum tube which contains an input window, a photocathode, focusing electrodes, an electron multiplier and an anode. They are usually sealed into an evacuated glass tube. Fig. 2.1 shows the schematic structure of a photomultiplier tube. Photon passes through the input window and excites electrons out in the photocathode by photoelectric effect. These electrons are referred to as photoelectrons. Photoelectrons are accelerated and focused by the focusing electrode onto the first dynode. Then they are multiplied on dynode by the secondary electron emissions process. These secondary emissions are repeated at each successive dynode. Then, the multiplied secondary electrons emitted from the last dynode are finally collected by the anode. The output is a current, not a voltage. Hence we need to connect a proper resistance to make a potential drop if we want to take the signal by a scope. This section describes the principle of photoelectron emissions, electron trajectory and the design of electron multiplier.

Photoelectron emission

We can roughly separate the photoelectron emission into two types, external and internal. The internal emission corresponds to photoelectrons being excited into conductive band of material. The photoca-

thode is referred to the external which represents the photoelectrons are emitted into vacuum from a material.

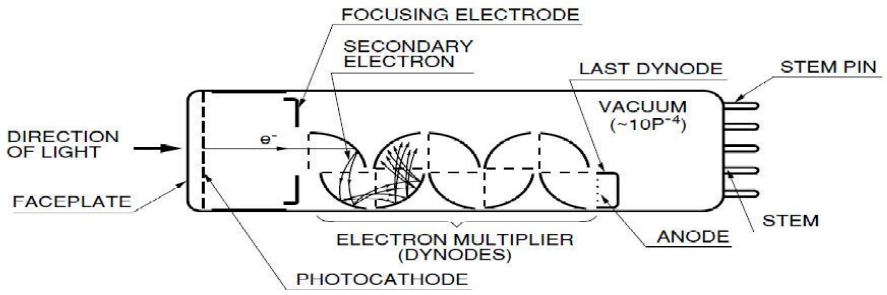

Fig. 2.1: Structure of a photomultiplier tube

Electron trajectory

In order to collect photoelectrons and secondary electrons efficiently on a dynode and also to minimize the electron transit time consumption, electrode design must be optimized through an analysis of the electron trajectory. Electron movement in a photomultiplier tube is influenced by the electric field which is dominated by the electrode configuration and the voltage applied to the electrode. The high-speed, large-capacity computers have come into use for numerical analysis of the electron trajectory. This method divides the area to be analyzed into a grid-like pattern to give boundary conditions, and obtains an approximation by repeating computations until the error converges to a certain level. By solving the equation of motion based on the potential distribution obtained using this method, the electron trajectory can be predicted[4].

Electron multiplier

As stated above, the electrode structure of a photomultiplier tube is designed to provide optimum performance. Photoelectrons emitted from the photocathode are multiplied from the first dynode till the last dynode, with electron amplification ranging from 10 to as much as 10^8 times, and are finally sent to the anode. For a primary electron hitting the surface of a dynode, the dynode nay emit *n* secondary electrons. This *n* is called the secondary emission ratio, representing the number of electrons generated

from a primary electron. Ideally, the gain is n^m for a photomultiplier tube with *m* dynode stages and the average secondary emission ratio *n* per stage [4].

Anode

The anode of a photomultiplier tube is an electrode that collects secondary electrons multiplied in the cascade process through multi-stages dynodes and outputs the electron current to an external circuit[4].

2.2 Response function

In this section, I introduce the response function of PMT which was proposed by E.H. Bellamy et al.[5]. I apply the function to fit the LED spectra and dark noise spectra. Weak light source is the basis for the function. LED intensity can be controlled easily by a pulse generator, so that its spectra can be understood by the response function.

A model of photomultiplier response

The response function consists of photon conversion, electron collection, amplification and background noise. The first two processes convert photons into electrons. The amplification describes how the initial electron is amplified. Finally the background noise is constructed from a general assumption.

Photo conversion and electron collection

Let us suppose that *I* is a source of light pulse with controllable frequency and intensity. The incident light on the photocathode produces photoelectrons via photoelectric effect. In practical case, the events of photons hitting the photocathode and transforming to photoelectrons are not a constant but following binomial distribution

$$P(n) = \frac{N!}{n!(N-n)!}(1-p)^{N-n}\,p^n \tag{2.1}$$

Where *P* is the probability of photon being caught by PMT and becoming photoelectron collected by the dynode system and *N* is total emitted photon by LED. The *p* is correlating with the size of PMT

window and quantum efficiency of photocathode.

If the light source is luminant for a while, one can imagine that plenty of photons, referred to as *N*, have been emitted. In the condition that *N*>>1, the binomial distribution approaches to Poisson distribution,

$$\begin{aligned} P(n) &\approx \lim_{N>>1} \frac{N!}{n!(N-n)!}(1-p)^{N-n}\, p^n \\ &\approx \lim_{N>>1} \frac{N!}{n!(N-n)!}(1-\frac{Np}{N})^{N-n}\, \frac{(Np)^n}{N^n} \\ &\approx \frac{\mu^n}{n!} e^{-\mu} \end{aligned} \tag{2.2}$$

where $\mu=Np$[5]. The μ, the mean number of collected photoelectrons, is determined by the mean number of photon hitting the photocathode, the photocathode quantum efficiency and the collection efficiency of the dynode system[5].

A PMT always possess extremely high current gain and rapid reaction time. If there are a huge number of photons passing through the PMT suddenly, a sharp current will be induced in the electronic system. It is like a lightning hitting the system and damaging it. So we need to be careful when we adjust the intensity of light source.

Amplification

Let us start from the simplest situation that there is just one photoelectron hitting the first dynode and the dynode produces g_1 electrons, which is the so called secondary electron emission. These electrons proceed to hit the second dynode and produce n_1g_2 electrons by binomial process. Here n_i is electron number picked up by each dynode and g_i is the gain coefficient for each dynode. The groups of electrons between dynodes are independent because the number of electrons in one group was determined by one dynode at each stage. Therefore, the distribution of *K* events is mainly determined by the final stage. This follows again, a binomial distribution.

$$G(x) = \frac{K!}{x!(K-x)!}(1-\rho)^{K-x}\rho^x \tag{2.3}$$

where ρ is the probability of an electron in the final stage being excited to the escape energy, *K* is total valence electrons on the dynode. Usually, *K* is very huge (>10^6) and ρ almost remains the same for each

valence electron. For K>>1, a binomial distribution approaches to a Gaussian.i.e.,

$$\lim_{K\gg 1} G(x) = \lim_{K\gg 1} \frac{K!}{x!(K-x)!}(1-\rho)^{K-x}\rho^{x}$$

$$\approx \frac{1}{\sqrt{2\pi}\sigma_1}\exp[-\frac{(x-Q_1)^2}{2n\sigma_1^2}] \ , \qquad (2.4)$$

where x the charge variable, $Q_1=K\rho$ is the average charge at the PMT output when one electron is collected by the first dynode, $\sigma_1 = \sqrt{K\rho(1-\rho)}$ is the corresponding standard deviation of the charge distribution[5]. The case of multi-electron distribution can be derived from formula (2.4) with the assumption that the amplification processes of charges initiated by different photoelectrons are mutually independent. The charge distribution of n photoelectrons, is a convolution of n one-electron case[5] such that

$$G_n(x) = \frac{1}{\sqrt{2\pi n}\sigma_1}\exp[-\frac{(x-nQ_1)^2}{2n\sigma_1^2}] \ . \qquad (2.5)$$

Note that this distribution has a correct limit for $n\to 0$

$$G_0(x) = \delta(x) \qquad (2.6)$$

where $\delta(x)$ is the delta function. This condition ensures that the output current is zero if there is no photon undergoing the amplification.

Hence, the response of an ideal PMT (no noise) can be found. It is simply a convolution of distributions in (2.2) and (2.5)

$$S_{ideal}(x) = P(n;\mu)\otimes G_n(x)$$

$$= \sum_{n=0}^{\infty}\frac{\mu^n e^{\mu}}{n!}\frac{1}{\sqrt{2\pi n}\sigma_1}\exp[-\frac{(x-nQ_1)^2}{2n\sigma_1^2}] \ . \qquad (2.7)$$

Background processes

We shall split the background process into two groups with different distribution functions:

(I)The low charge processes present in each event such as leakage current, etc, which are responsible

for nonzero width of the signal distribution when no photoelectron was emitted from the photocathode. This process is called pedestal[5].

(II)The discrete processes which accompany the measured signal such as thermo-emission, noise initiated by the measured light, etc[5].

Type I processes can be described by a Gaussian while type II processes can be described by an exponential function. The effect of these processes when some primary photoelectrons (*n* greater than one) are emitted will be discussed later. When no primary photoelectron is emitted (*n* = 0, with probability $e^{-\mu}$), only type I and II processes occur. If we call *w* the probability that a background signal of type II can occur, we can parameterize the background as

$$B(x) = \frac{(1-w)}{\sigma_0\sqrt{2\pi}}\exp(-\frac{x^2}{2\sigma_0^2}) + w\theta(x)\alpha\exp(-\alpha x) \tag{2.8}$$

Where σ_0 is the standard deviation of type I background distribution, *w* is the probability that a measured signal is accompanied by a type II background process, α is the coefficient of the exponential decrease of type II background, $\theta(x)$ is the step function[5].

The realistic response function of the PM

Taking into account the ideal PMT spectrum (2.5) and the background charge distribution (2.8), we find that the realistic PMT spectrum is given by the convolution:

$$\begin{aligned} S_{real}(x) &= \int S_{ideal}(y)B(x-y)dy \\ &= \sum_{n=0}^{\infty}\frac{\mu^n e^{-\mu}}{n!}\left[g_n(x-Q_0) + wI_{G_n\otimes E}(x-Q_0)\right] , \end{aligned} \tag{2.9}$$

with

$$g_n(x-Q_0) = \frac{1-w}{\sigma_n\sqrt{2\pi}}\exp\left[-\frac{(x-Q_n)^2}{2\sigma_n^2}\right] , \tag{2.10}$$

$$I_{G_n\otimes E}(x-Q_0) = \int_{Q_0}^{x} G_n(y-Q_0)\alpha\exp\left[-\alpha(x-y)\right]dy \tag{2.11}$$

$$= \left[erf\left(\frac{x-Q_n-n\sigma_1^2\alpha}{\sigma_1\sqrt{2n}}\right) + erf\left(\frac{\left|Q_0-Q_n-n\sigma_1^2\alpha\right|}{\sigma_1\sqrt{2n}}\right)\right]$$

$$\times \frac{\alpha}{2}\exp\left[-\alpha\left(x-Q_n-\frac{n\alpha_1^2\alpha}{2}\right)\right], \tag{2.12}$$

$$Q_n = Q_0 + nQ_1 ,$$

$$\sigma_n = \sqrt{\sigma_0^2 + n\sigma_1^2} \tag{2.13}$$

Hence Q_0 is the pedestal and erf(x) is the error function. The meanings of other parameters are the same as those in (2.2), (2.5) and (2.8). $g_n(x)$ is now a convolution of the ideal n photoelectrons charge distribution of PMT (2.7) with the Gaussian part of background (2.8). The standard deviation associated with $g_n(x)$ is $\sqrt{\sigma_0^2 + n\sigma_1^2}$. In the zero photoelectron case, $g_n(x\text{-}Q_0)$ is not a delta function any more, but a Gaussian with standard deviation σ_0. Hence, $I_{G_n \otimes E}$ is reduced to α*exp[-α(x-Q_0)]/2.

In summary, the response function contains seven free parameters. Two of them Q_0 and σ_0 define the pedestal. Two others, w and α describe the background, and the remaining three parameters Q_1, σ_1 and μ are related the spectrum of the real signal. Of the three parameters, μ is proportional to the intensity of the light source, while Q_1 and σ_1 characterize the amplification process of the PMT dynode system[5].

In this chapter, I have introduced the structure and the response function of PMT. However in the real circumstance, it is not easy to perform fitting well with a function which contains seven free parameters. Hence in certain condition, we can fix a few parameters before performing the fitting for others. For example, w and α represent the background of PMT and they are close to zero for weak light in generally. Hence I first measured and fitted the pure background signal to get w and α. Besides, the magnitude of I term is much smaller than that of the Gaussian term. This means I can set w and α to zero without altering the fitting result too much even w and α are not so close to zero. Furthermore, n could be started from one rather than zero when I chose a suitable fitting range. This means that Q_0 and σ_0 can be taken as constants. With the above simplification, seven parameters are reduced to three, Q_1, σ_1 and μ. This simplifies our fitting process.

Chapter 3

The photomultiplier calibration

3.1 Motivation

In a neutrino oscillation experiment such as Daya Bay, the standard method for detecting neutrino signals is through collecting photon signals and reconstruct them to neutrino signals. Hence there are a lot of photomultiplier tubes inside each detector and water pool. However the gains of PMTs are not identical and they also vary with time. Therefore the gain calibration is an important task [3].

The PMT calibration in Daya Bay experiment is performed by two methods, one puts LED sources at several positions inside AD, another collects the dark noises of PMTs. The advantage of using the second method is that one does not need to shutdown the physics runs, so such that one can take physics data and perform calibration at the same time. Here I compared the gains of LED sources and those of dark noises[3].

3.2 The setup of experiment

I used the same PMT (Hamamatsu-R6236), electronic system and DAQ (NI PXI-5152) in both methods. The only difference between two methods is the setting of trigger sources. Fig. 3.1 and Fig. 3.2 are simple layouts of the settings[6,7].

Dark noise

It has been mentioned in Chapter 2 that the electrons at photocathode, dynodes and anode could be excited by thermo effect and high voltage effect, etc. They may be considered as external signals by DAQ

Fig. 3.1: The layout for gain calibration by dark noise. The two output signals are the same, but one is treated as the trigger source. This is the self-trigger method.

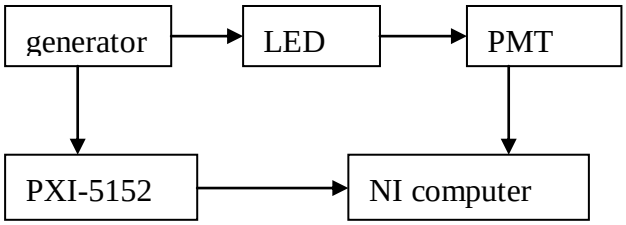

Fig. 3.2: The two output signals are generate by the generator periodically. One is used to drive the LED, another is used to open the time window by PXI-5152.

through the amplification process. Namely, even the PMT is placed in a perfectly dark box, there is still a little current flowing through it. This current is also called dark current.

First I connected a square plastic scintillator upon the faceplate of the PMT and covered it with aluminum film. I then wrapped it by black tape. Fig. 3.3 shows the appearance. When particles pass through the scintillator, they may interact with the scintillator and then emit gamma rays. For example, in neutrino oscillation experiment, the detectors collect photons from inverse beta-decay reaction. Thephoton signals can be used to infer the positions and energies of positrons and neutrons. This information is useful for reconstructing the energies of neutrinos. Because muon is the main source which interacts with the scintillator in our case, muon signal can be used as the random trigger. This method is useful not only because the muon rate is fast but also the error for mistaking muon signals as dark current can be reduced. The whole process begins when muons pass through the scintillator and emit photons. PMT receive photons, convert it to photoelectron and then amplifies the signal. Finally DAQ measures the output current of PMT and then takes the voltage as a trigger if it exceeds the threshold. Since I need only the dark noise, so I open a time window to record only dark noise. The time window has 200 nanoseconds width and prior to muon signals. Because the time window is used to record dark noise

especially, it is called noise window. These dark noise hits are basically single photo-electron signal and they can be used for gain fitting and hits rate calculation. We choose noise window prior to muon signal rather than posterior to it. This is because that the latter contains other signals such as ringing and afterpluses. This time window is not suitable to extract the dark noise. Fig. 3.4 is a typical TDC (time to digital converter) distribution. Table 3.1 shows some setups of DAQ. Basically, the resolution of voltage is $1/2^8$. For example, the voltage range is set to be 10V, so the resolution is $10/2^8$, namely 0.039. But actually, it still has the limit 0.008646.

Fig. 3.3: The setup for measuring the darknoise.

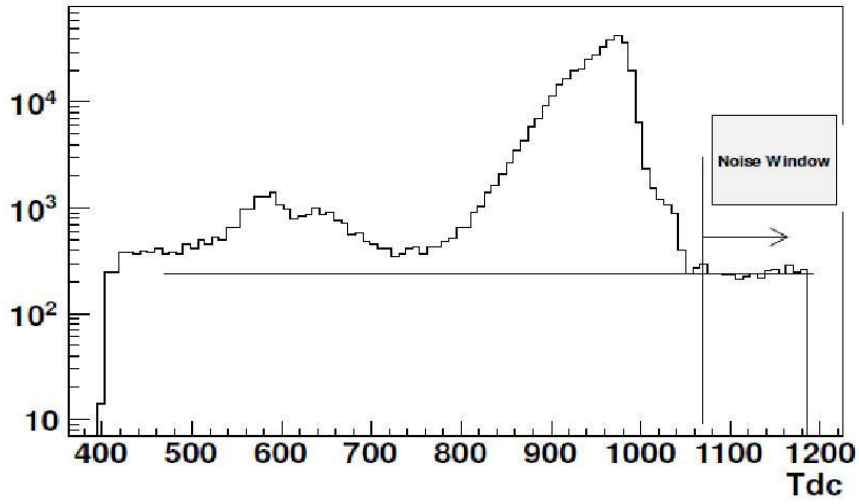

Fig. 3.4: A typical TDC distribution. The physics events happen around TDC 960. However the readout starts from 1190 to ensure all hits are enclosed. The window from 1070 to 1190 is called noise window.

width	200ns
sample rate	1G/s
resolution	8bits
trigger level	1.29Vpp
Voltage range	1.4Vpp

Table3.1: some setups and conditions of DAQ.

Pulse height spectra

When a signal is recorded by DAQ, its pulse shape appears like the one shown in Fig. 3.5. A pulse height is obtained by subtracting the average pedestal of every event from the pulse peak. In this method, Q_0 is no longer meaningful, even though it shows up in the fitting process. In I took twenty days of data for darknoise, and fit the data every day. Fig. 3.6 shows some of the fitted data.

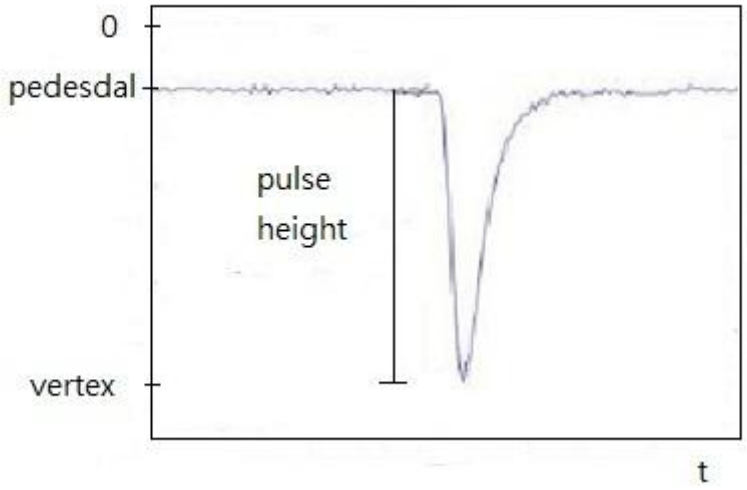

Fig. 3.5: The sketch of signal pulse. The pulse height is obtained by subtracting the average of pedestal from the pulse peak.

The twenty-day data were taken during 7/12 to 8/16 in 2012. During this period, I encountered some unexpected situation such as power failure and typhoon so that the system had to be shutdown. After

the problem was resolved, it took a day to warm up the machine and resume the data taking. Fig. 3.7 and Fig. 3.8 show the variation of Q_1 and the error range day by day. The definition of error range is

$$R_x = \frac{Q_x - Q_{ave}}{Q_{ave}} \times 100\% \tag{3.1}$$

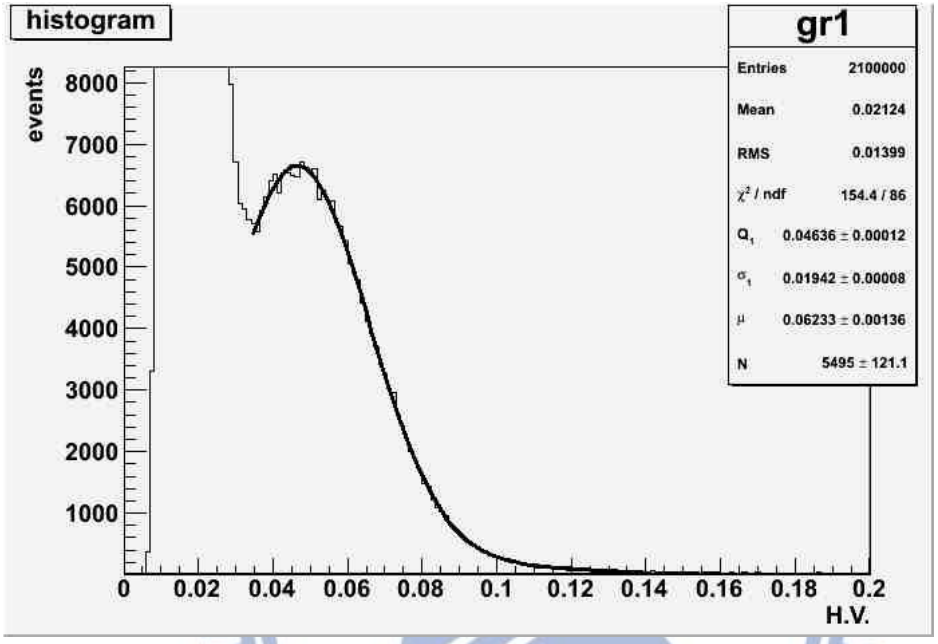

(a)

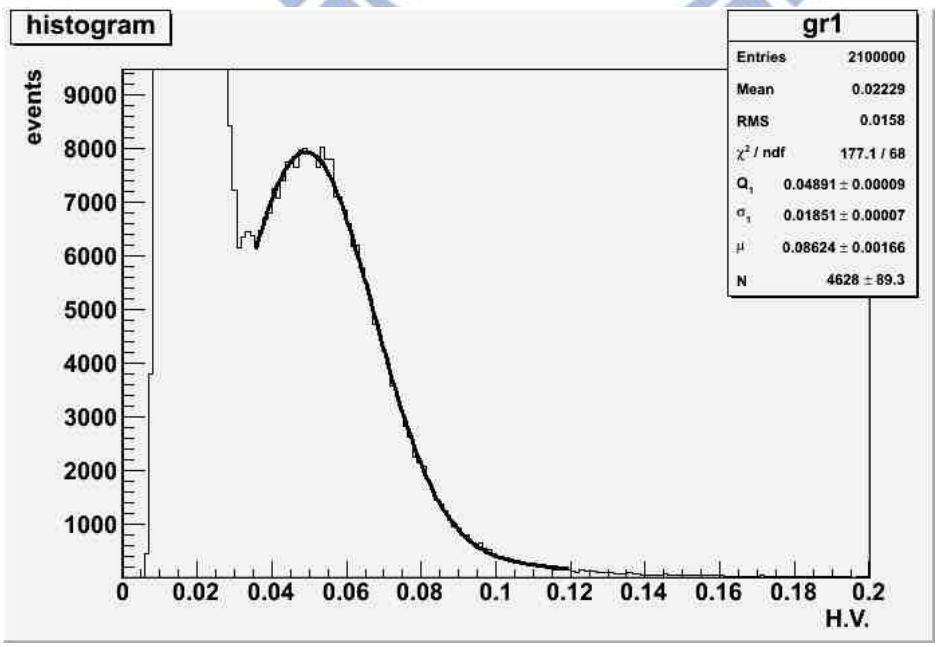

(b)

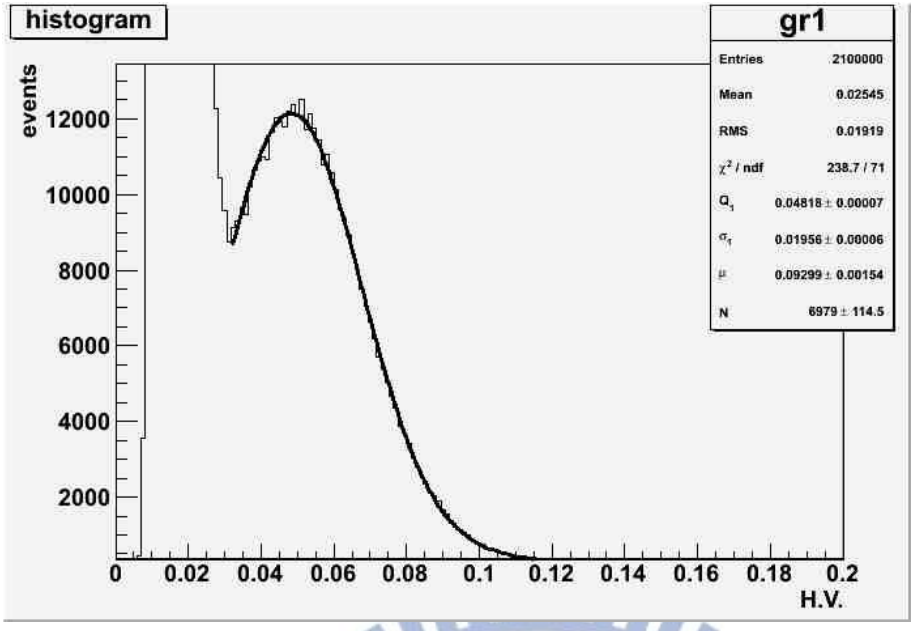

(c)

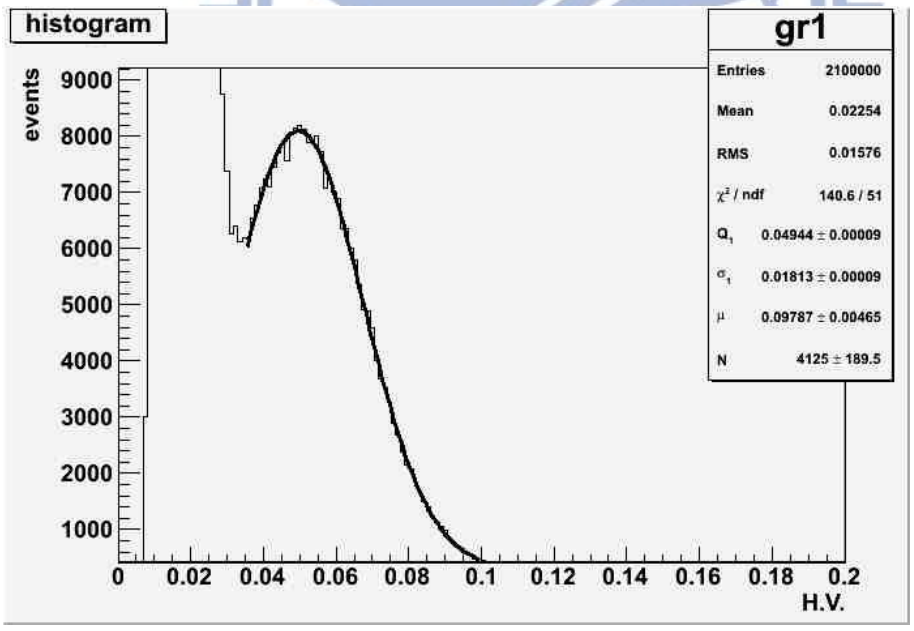

(d)

Fig. 3.6: each picture represents fitting result for data taken on each day.

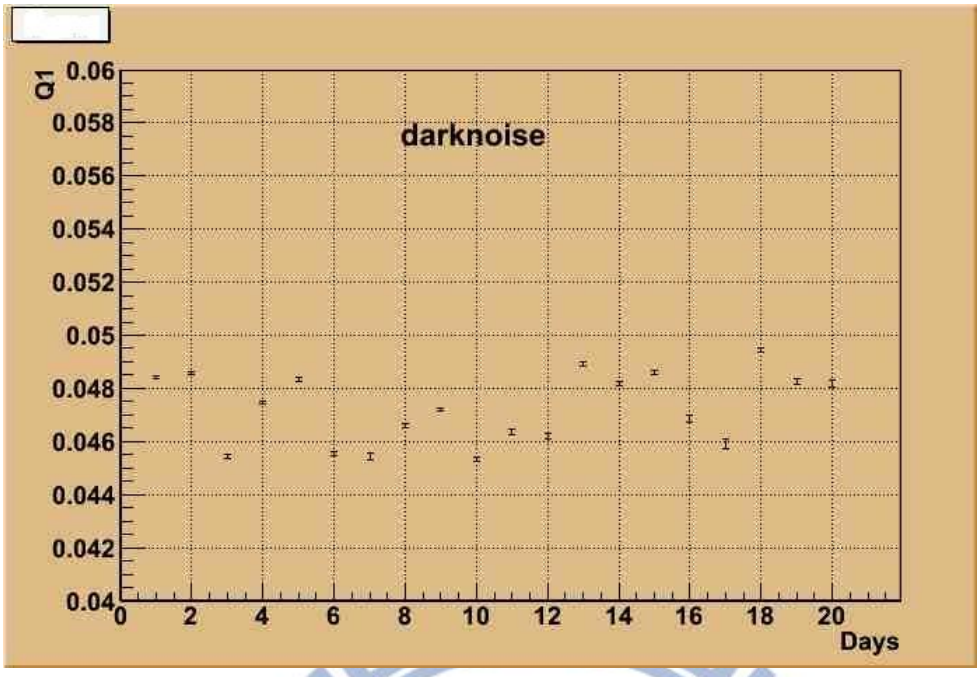

Fig. 3.7: The value of Q_1 one each day, the order of Q_1 is 10^{-2}.

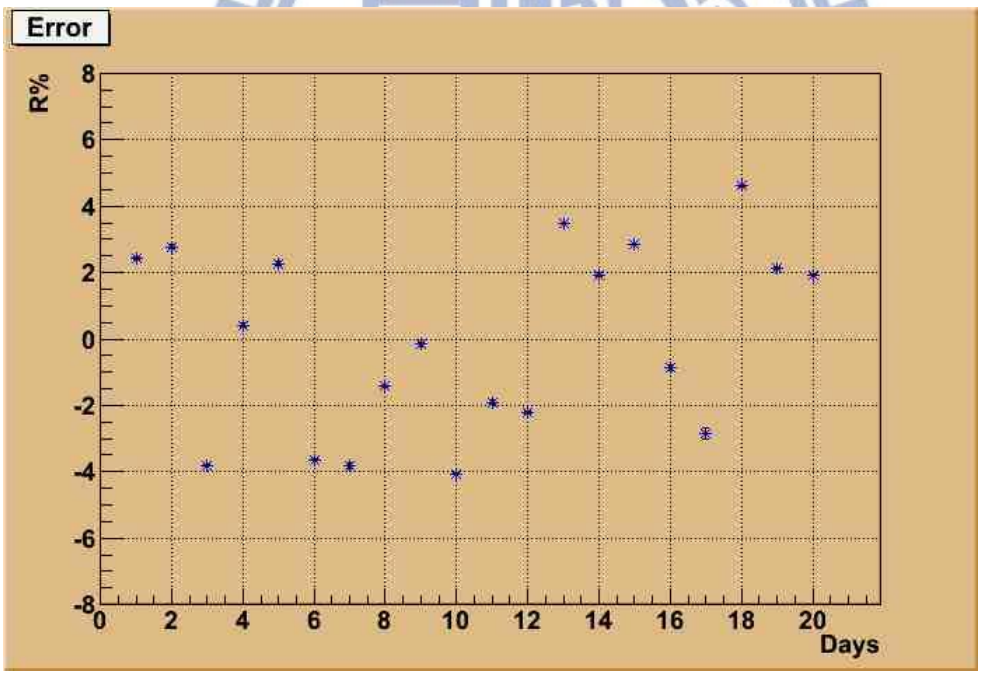

Fig. 3.8: The error range of Q_1.

Light source-LED

PMT is very sensitive to light source, even few photons can be detected. So a good black box for light source is needed. The box size is about 60 cm×30 cm×25 cm. It was made of wood and painted with opaque paint several times to reduce the possibility of reflection and penetration. The light source I

used is LED. The LED was connected with function generator. The function generator can control light source by sending square pulses to LED. The light intensity, frequency and width could be adjusted through function generator. The distance between PMT and LED is about 50 cm. Because the PMT has the most sensitivity in the range from 400 nm to 500 nm, I used the blue light LED. Fig. 3.9 shows the PMT and LED in the black box.

To begin, it is necessary to test the effect of black box. A black box without any light source in it was covered by a cloth, one side of the cloth is black and the other side is reflective. I then turned on the PMT for a while. One expects that the pulse height spectrum is a pure narrow Gaussian shape. Fig. 3.10 shows the actual pulse height spectrum of pedestal in my case.

After the test round and the warming up of apparatus, I set the frequency and width of the LED to be 20 kHz and 50ns, respectively. The pulse generator sends the signal to LED and a square-wave function to DAQ as trigger simultaneously. The pulse height is from 2.45V to 2.50V. When DAQ receives the square-wave function, it opens a posterior 200ns width. The duration of the whole process which begins from photon emission from the LED and ends at the recording of output voltage by DAQ is about 100ns.

The fitting method is the same as the darknoise part. Fig. 3.11 shows some fitted results. Fig. 3.12 and Fig. 3.13 shows the error range and trend of Q_1.

The LED data taking period includes a transition from the old building to the new one. Hence I took the data at two different locations. I separated them into LED-old and LED-new. Fig. 3.15 and Fig. 3.16 shows the error range and the trend of Q_1.

Fig. 3.9: The PMT was placed on the right side, LED was attached to the black stick on the left side.

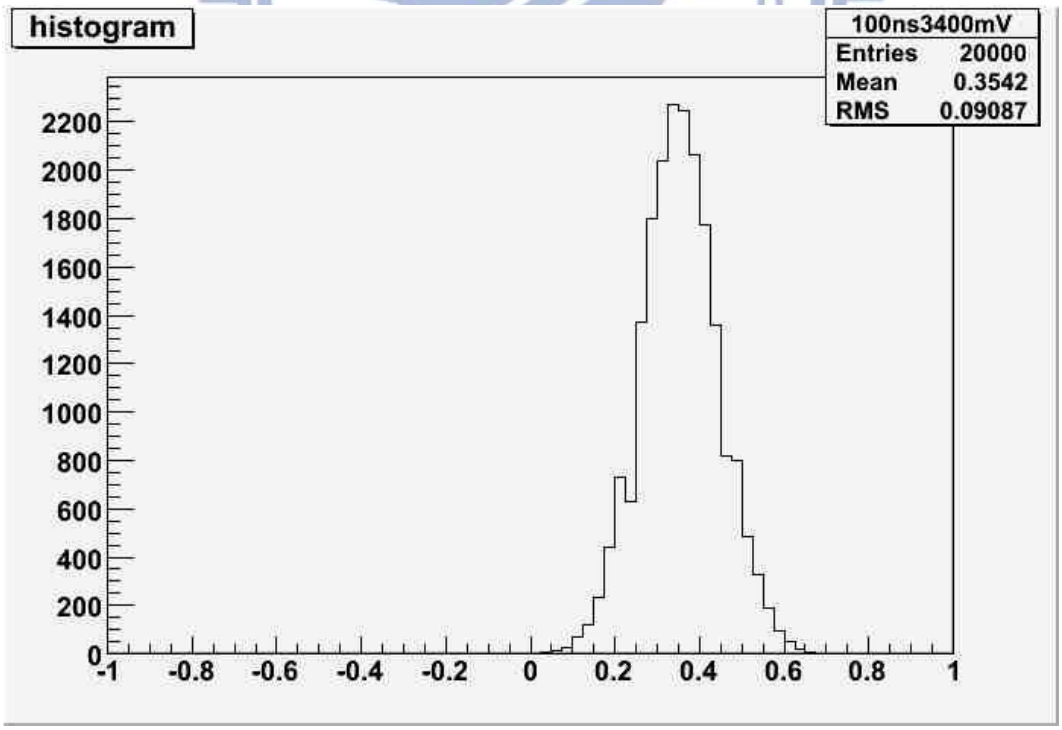

Fig. 3.10: The pulse height spectrum of pedestal.

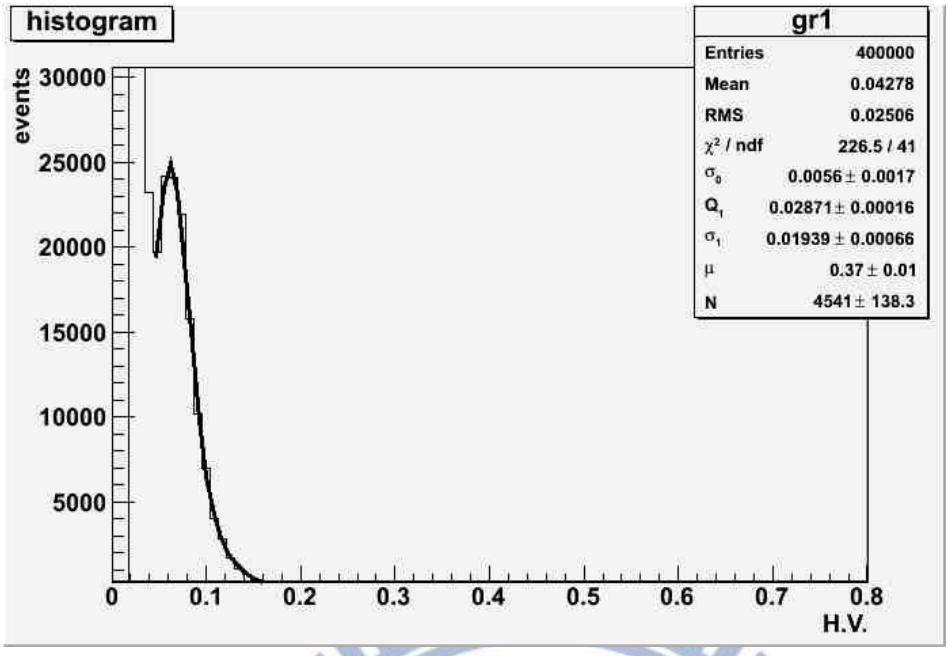
histogram
gr1
Entries 400000
Mean 0.04278
RMS 0.02506
χ² / ndf 226.5 / 41
σ0 0.0056 ± 0.0017
Q1 0.02871 ± 0.00016
σ1 0.01939 ± 0.00066
μ 0.37 ± 0.01
N 4541 ± 138.3
events
30000
25000
20000
15000
10000
5000
0
0.1
0.2
0.3
0.4
0.5
0.6
0.7
0.8
H.V.

(a)

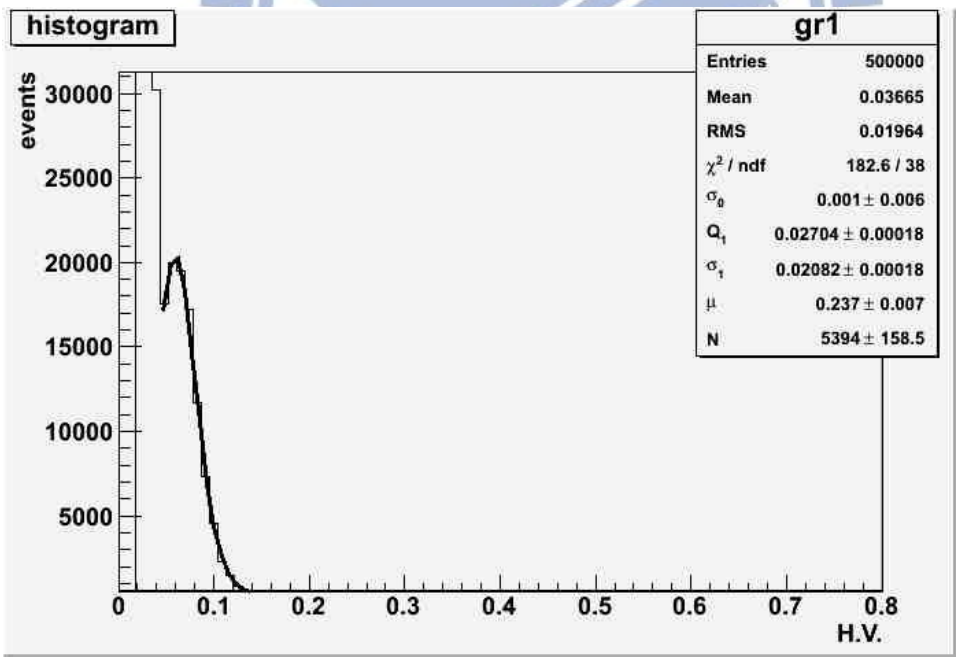
histogram
gr1
Entries 500000
Mean 0.03665
RMS 0.01964
χ² / ndf 182.6 / 38
σ0 0.001 ± 0.006
Q1 0.02704 ± 0.00018
σ1 0.02082 ± 0.00018
μ 0.237 ± 0.007
N 5394 ± 158.5
events
30000
25000
20000
15000
10000
5000
0
0.1
0.2
0.3
0.4
0.5
0.6
0.7
0.8
H.V.

(b)

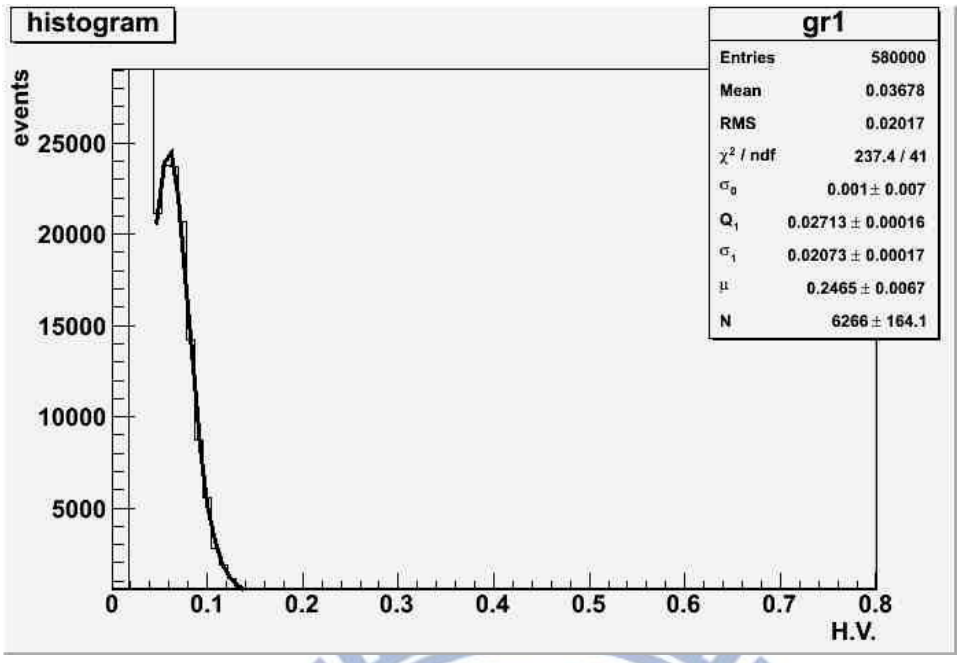

(c)

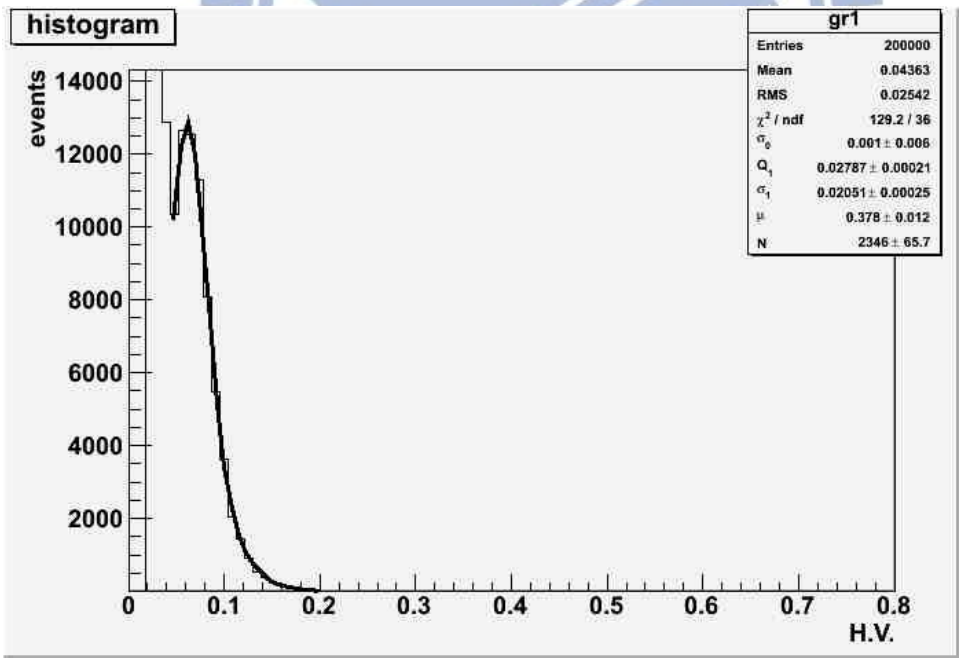

(d)

Fig. 3.11: Some fitted data obtained by the LED method.

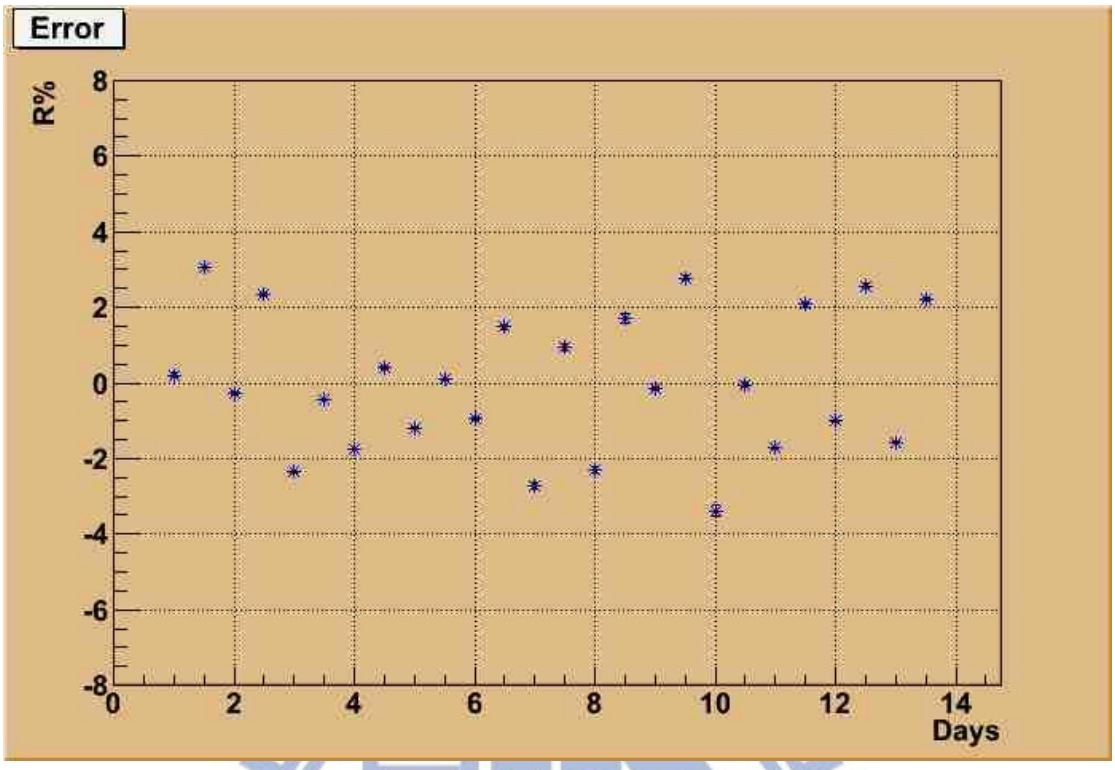

Fig. 3.12: The error range of Q_1. The data was taken from Aug. 17 to Aug. 30..

Fig. 3.13: The Q_1 value of LED-old. The horizontal axis starts from 21, which means the LED run is a continuation of 20-day darknoise run..

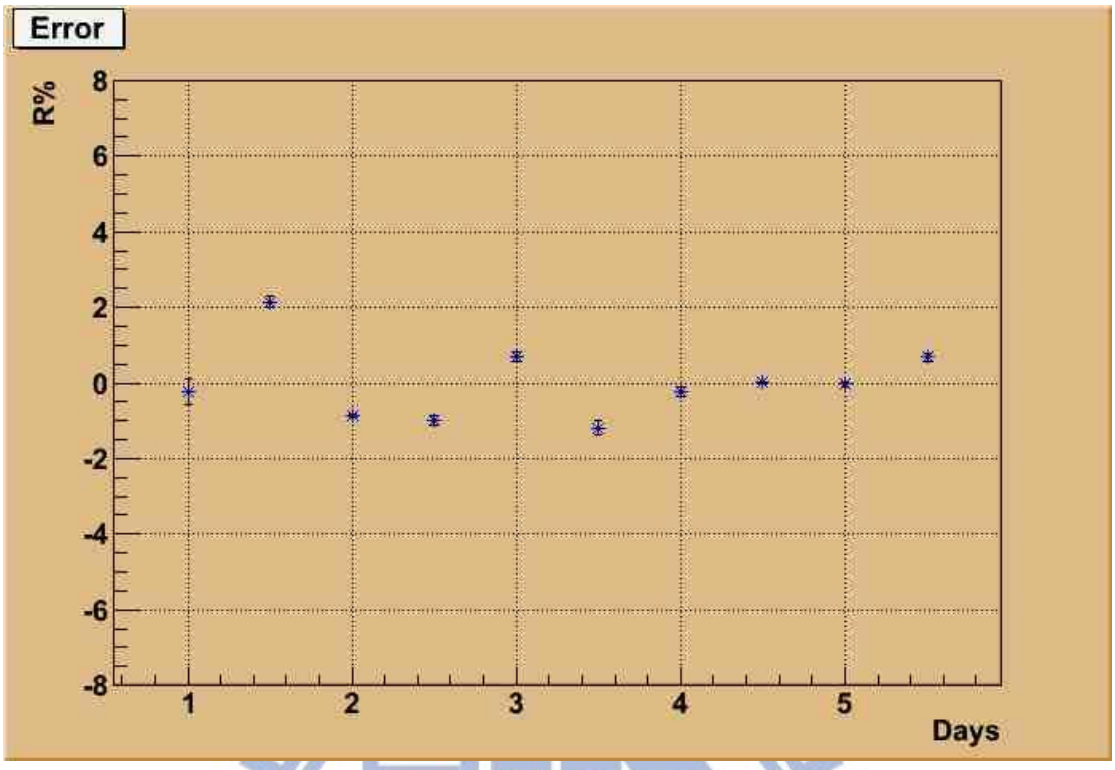

Fig. 3.14: The error range of Q_1 of LED-new.

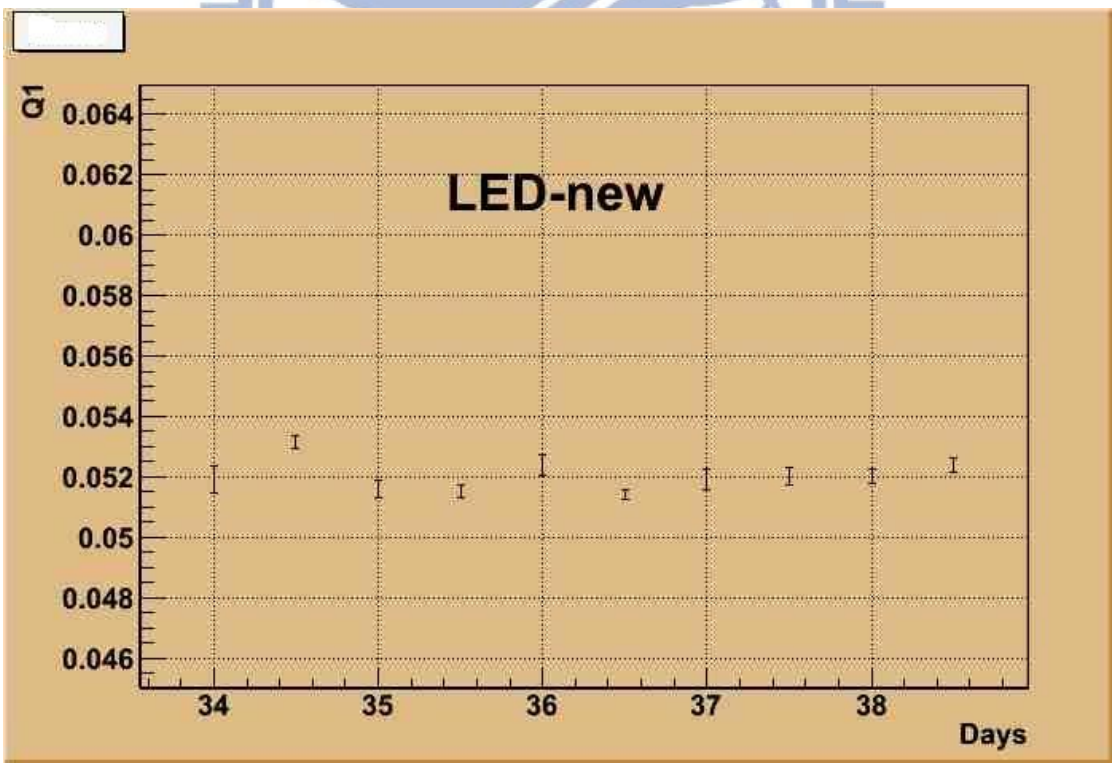

Fig. 3.15: The Q_1 value of LED-new.

Result

Now we compare Q_1 obtained by two methods and calculate the difference between them. Table 3.2 shows the maximum, minimum, average and error range of Q_1. First we only discuss the darknoise and LED-old which were taken at the same place. We find that the minimum and average of Q_1 are very close. The maximum Q_1 of darknoise is larger than the one of LED-old by 0.00105. It is much larger than Q_1 obtained the other days. If the value 0.04944 is treated as unusual, the re-calculated result of darknoise is much more consistent with LED-old. No matter we disregard the value 0.0494 or not, the result shows that using the two methods to do calibration is feasible. The difference between the two methods is less than 0.7%. Fig. 3.17 puts the Q_1 of the two methods abreast.

	minimum	maximum	average	R%
Darknoise	0.0453	0.0494	0.0473	-4%~4.6%
	0.0453	0.0489	0.0471	-3.8%~3.7%
LED-old	0.0454	0.0484	0.0469	-3.3%~3%
LED-new	0.0514	0.0531	0.0520	-1.2%~2.1%

Table 3.2: Q_1 values obtained by two methods. The first row of darknoise is the whole twenty-day data and the second one is the nineteen-day data which subtracts the odd one-0.04944.

The Q_1 spread is wide for one PMT. However, if there are multi-PMTs which are calibrated at the same time, this produces a distribution of Q_1. Then the weighted average of Q_1 can give a better accuracy[8]. Suppose we have a set of n independent measurements, x_i. If the x_i have different, known variances σ_i^2, then the weighted average

$$\mu = \frac{1}{w}\sum_{i=1}^{n} w_i x_i \qquad (3.2)$$

Here $w_i = 1/\sigma_i^2$ and $w = \sum_i w_i$. The standard deviation of μ is $1/\sqrt{w}$.

For example, in Daya Bay experiment, there are 192 PMTs in AD. If all these PMTs are good and the variance of PMT is close to each other. Hence the Q_1 values of these 192 PMTs form a Gaussian distribution. The weighted mean of Q_1 is more accurate than each individual Q_1 by $\sqrt{192}$ times.

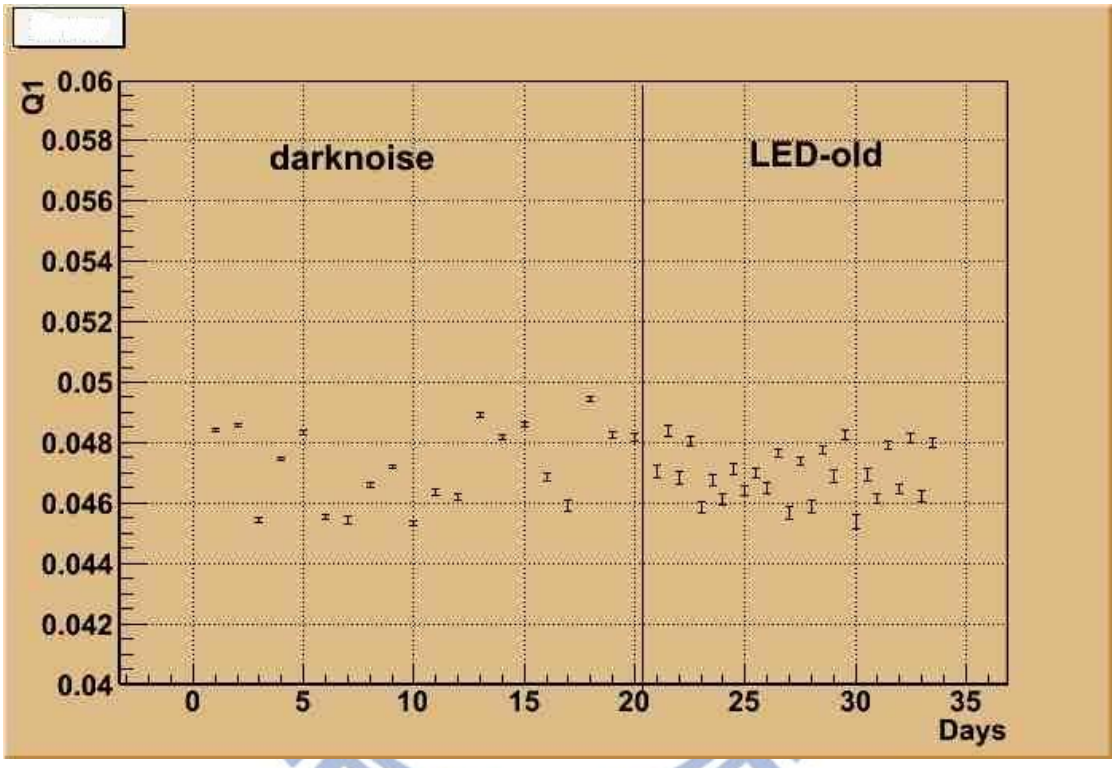

Fig. 3.16: Q_1 obtained by two methods on each day are shown.

We can see that the Q_1 of LED-new is more stable and higher than that of LED-old, though the former was just taken for a few days. The reason is probably that the old building is not built for doing experiment, hence its power supply and electrical system are not well grounded. This means the experiment is easily fluctuated due to external interference.

Unfortunately, the high voltage supply was set to be 1400V, and I could not measure and record the actual voltage. Hence I cannot confirm the conjecture.

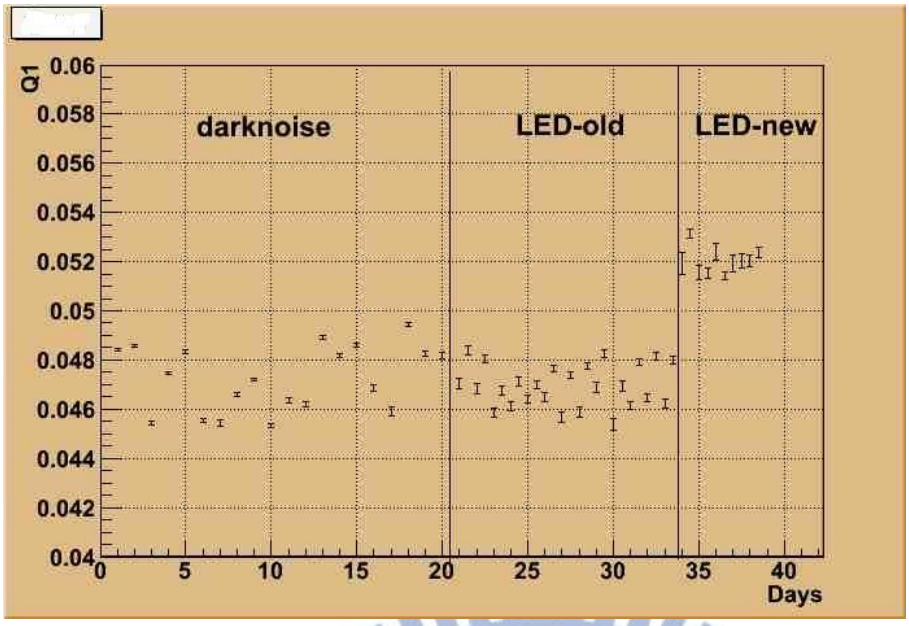

Fig. 3.17 : the total trend of Q_1. The darknoise and LED-old were taken in old building, the LED-new was taken in the new building.

High-intensity light

In order to ensure the fitting function is reasonable, I also use the same function to fit high-intensity light spectrum. Fig. 3.18 shows the fitting result of high-intensity light level which μ is larger than four. The difference of Q_1 between high-intensity light level and low-intensity light level is about 10%. It seems that the parameter condition of low light level is not precisely the same as that of high-intensity light level, but it is reasonable.

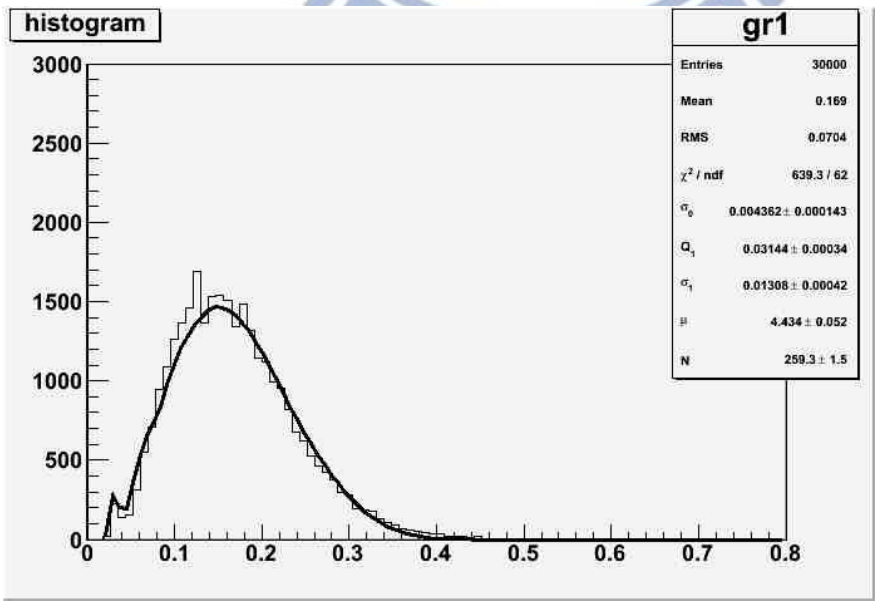

Fig. 3.18:The fitting spectrum of high-intensity light(μ>4).

Chapter 4

Summary

I spent 33 days to calibrate the PMT which consist of 20 days with the darknoise method and 13 days with the LED method. I obtained 20 Q_1 from the darknoise and 26 Q_1 from the LED. The results show that gains obtained by darknoise and LED methods are consistent. The difference between the two methods is less than 1%. The weighted mean of Q_1 taken from multi PMTs has a lower fluctuation than the one with respect to single PMT. Since the PMT gain can be easily affected by environment and apparatus, we need to monitor the PMT gains all the time.

All IAVs have been installed in ADs and physical runs have been taken. The Daya Bay team has published the collaboration's first result on $\sin^2 2\theta_{13}$ in March 2012 and has updated the result recently[10][11].

Bibliography

[1] W-M Yao et al. (Particle Data Group). *Journal of Physics G: Nuclear and Particle Physics Vol33 July 2006 Pp1-1232 Review of Particle Physics*. Institute of Physics, 2006.

[2] F. A. Scott. *Energy spectrum of the beta rays of radium* e. Phys. Rev., 48(391), 1935.

[3] Daya Bay collaborators. *Technical Design Review*, second edition, 2008.

[4] Hamamatsu Photonics K.K., photomultiplier Tubes – Basics and Applications, 2006.

[5] E.H. Bellamy et al., *Absolute calibration and monitoring of a spectrometric channel using a pho tomultiplier.* Nucl. Instr. And Meth. A 339(3), p.468, 1982.

[6]http://sales.hamamatsu.com/en/products/electron-tube-division/detectors/photomultiplier-tubes/part r6236-01.php

[7] http://sine.ni.com/nips/cds/view/p/lang/zht/nid/203069

[8] Particle Data Group. *Statistics*. 2011.

[9] 何泰祥，”*大亞灣微中子探測器與香港仔中子探測器研究*”，國立台灣大學，碩士論文，2009。

[10] Daya Bay collaborators. *Observation of electron-antineutrino disappearance at Daya Bay*, Phys. Rev. Lett. 108, 2012.

[11] Daya Bay collaborators. *Improved Measurement of Electron Antineutrino Disappearance at Daya Bay*, arXiv:1210.6327.

[12] Daya Bay collaborators. *A side-by-side comparison of Daya Bay antineutrino detectors*, Nucl. Instr. Meth A 685, 78-97, 2012.